First-Principles Study on the Grain Boundary Embrittlement of Metals by Solute Segregation: Part II. Metal (Fe, Al, Cu)-Hydrogen (H) Systems

MASATAKE YAMAGUCHI, KEN-ICHI EBIHARA, MITSUHIRO ITAKURA, TOMOKO KADOYOSHI, TOMOAKI SUZUDO, and HIDEO KABURAKI

The microscopic mechanism of grain boundary (GB) embrittlement in metals by hydrogen segregation (trapping) has been not well understood for many years. From first-principles calculations, we show here that the calculated cohesive energy of bcc Fe $\Sigma3(111)$ and fcc Al(Cu) $\Sigma5(012)$ symmetrical tilt GBs can be significantly reduced if many hydrogen atoms segregate at the GBs. This indicates that the reduction of the cohesive energy of the GB may cause the hydrogen-induced GB embrittlement in Fe, Al, and Cu. Considering the "mobile" effect of hydrogen during fracture, especially for the Fe system, more hydrogen atoms coming from solid solution state can segregate on the gradually formed two fracture surfaces and reduce further the cohesive energy. We suggest a new idea about the upper and lower critical stresses observed in the constant-load test of hydrogen-induced delayed fracture in high-strength steels; the upper critical stress is determined by the amount (density) of "immobile" hydrogen atoms segregated at the GB before fracture, and the lower critical stress is determined by the total amount (density) of immobile and mobile hydrogen atoms, the latter of which segregate on the two fracture surfaces during fracture.

I. INTRODUCTION

IN Part I,[1] we calculated the change in the cohesive energy of bcc Fe $\Sigma3(111)$ symmetrical tilt grain boundary (GB), $2\gamma_{int}$, by solute (B, C, P, and S) segregation. We found that the rate of the increase/decrease in the calculated $2\gamma_{int}$ with increasing segregation was proportional to the experimentally observed shift in the ductile-to-brittle transition temperature of high-purity iron with increasing segregation. This indicates that the change in the $2\gamma_{int}$ plays a key role in the GB embrittlement of metals as suggested by Rice and Wang.[2] In this part, we investigate hydrogen embrittlement of metals in the same way.

Generally speaking, the reduction of the cohesive energy of GB by hydrogen segregation is not considered as a key factor in the mechanism of hydrogen embrittlement of metals.[3] This is partly because it is not known how many hydrogen atoms can segregate at GBs of metals and how much the cohesive energy (work of fracture) of the GB can be reduced by the hydrogen segregation. The reduction of the cohesive energy of iron GB by hydrogen is inferred by Zhong et al. from first-principles calculations for the first time.[4] However, they did not determine the segregation atomic site for hydrogen from the calculations of the segregation energy, and did not calculate the cohesive energy itself. On the other hand, the interactions between vacancy and hydrogen in metals have recently attracted much attention. Experimentally, it has been recently found that hydrogen enhances vacancy formation in metals.[5] For this reason, some recent theoretical (first-principles) works focus on the vacancy-hydrogen interactions and discuss the relation with hydrogen embrittlement.[6,7] However, these works cannot explain the reduction of fracture stress based on fracture mechanics.

In this part, we calculate the segregation energy of hydrogen atom at the GB and its fracture surfaces for bcc Fe $\Sigma3(111)$ and fcc Al (Cu) $\Sigma5(012)$ symmetrical tilt grain boundaries (STGBs). From the GB and fracture-surface segregation energies of hydrogen, we calculate the change of $2\gamma_{int}$.[8] We show that the cohesive energy of the GBs of Fe, Al, and Cu can be significantly reduced if many hydrogen atoms segregate at GBs and fracture surfaces.

In this study, the effect of surface diffusion of hydrogen atom on the fracture surfaces and the mobile effect of hydrogen atom from solid solution state to the gradually formed fracture surfaces are discussed. By considering both the mobile and immobile effects of hydrogen atom, we suggest a new idea about the upper and lower critical stresses in the constant-load tests of delayed fracture induced by hydrogen in high-strength

MASATAKE YAMAGUCHI and HIDEO KABURAKI, Senior Researchers, and KEN-ICHI EBIHARA, MITSUHIRO ITAKURA, TOMOKO KADOYOSHI, and TOMOAKI SUZUDO, Researchers, are with the ("Fundamental Studies on Technologies for Steel Materials with Enhanced Strength and Functions" Consortium of JRCM), Center for Computational Science and e-systems, Japan Atomic Energy Agency, Tokai-mura, Ibaraki-ken, 319-1195 Japan. Contact e-mail: yamaguchi.masatake@jaea.go.jp
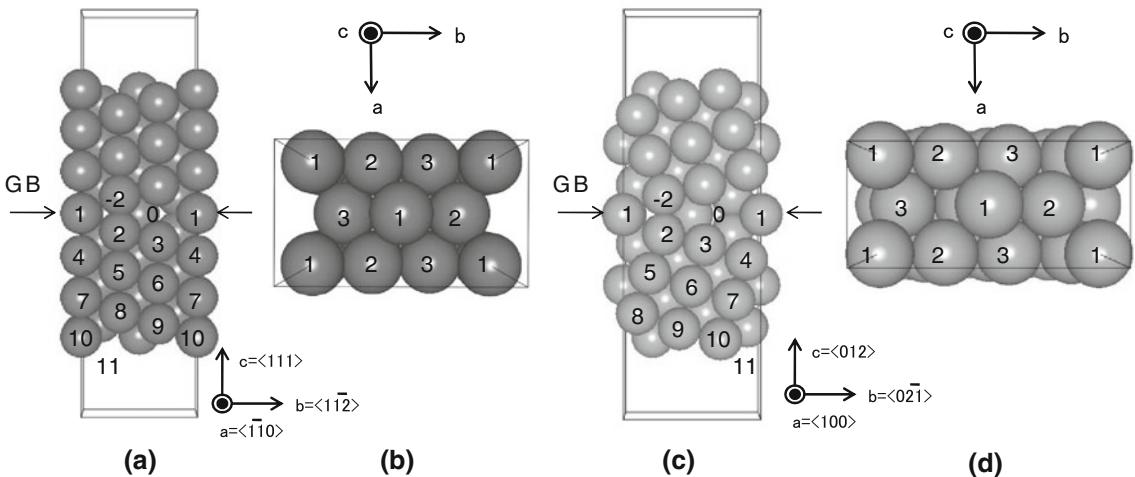
Fig. 1—Unit cell modeling of bcc Fe Σ3(111) and fcc Al(Cu) Σ5(012) STGBs. (*a*) Side view of bcc Fe Σ3(111) STGB. (*b*) Top view of the GB fracture (111) plane of bcc Fe Σ3(111) STGB. (*c*) Side view of fcc Al(Cu) Σ5(012) STGB. (*d*) Top view of the GB fracture (012) plane of fcc Al(Cu) Σ5(012) STGB. Atomic sites are denoted by numbers. The interstitial atomic sites are not shown for simplicity. The GB fracture planes in (*b*) and (*d*) have the same structure as the free surface planes in (*a*) and (*c*), respectively.

steels. The concept of upper and lower critical stresses are shown in Figure 1 of Reference 9. The upper critical stress is defined as the lowest fracture stress at which the fracture occurs without any delay time after an incubation period. Here, the incubation period is the time that is necessary for microcrack initiation. In other words, the cracks propagate very fast just after the incubation period at the upper critical stress. On the other hand, the lower critical stress is defined as the lowest fracture stress at which fracture occurs after very long delay time; the delayed fracture cannot occur at the stress that is smaller than the lower critical stress. To our knowledge, no one has ever explained the physical origin of the upper and lower critical stresses from when Troiano[9] suggested the concept in 1960, although there are many theoretical models of hydrogen embrittlement.

II. CALCULATIONS

A. *Modeling of GB, Fracture-Surface/GB Segregation Energy*

The calculation procedure is almost the same as that in Part I,[1] except for the calculation of the cohesive energy of GB ($2\gamma_{int}$). The unit cell including bcc Fe Σ3(111) STGB is shown in Figures 1(a) and (b). The tilt angle is 70.5 deg, and the rotation axis is $\langle 1\bar{1}0 \rangle$. In the upper and lower regions of this cell, we introduce a vacuum region to allow GB sliding along the GB plane. We chose this GB because the structure is simple but the GB energy is relatively high. For the calculations of B, C, P, and S segregation at bcc Fe Σ3(111) STGB in Part I,[1] we use the unit cell that includes 76 Fe atoms. For the calculations of hydrogen segregation at bcc Fe Σ3(111) STGB in this part, on the other hand, we use the unit cell whose size is half in the *a*-axis direction, as shown in Figures 1(a) and (b), which includes 36 Fe atoms. We use this half-size cell to reduce computational time. For the cases of fcc Al(Cu)-H systems, we chose

fcc Σ5(012) STGB, because the structure of fcc Σ5(012) STGB is very close to that of bcc Fe Σ3(111) STGB. The unit cell including fcc Σ5(012) STGB is shown in Figures 1(c) and (d), whose cell size and structure are very close to the cell including bcc Fe Σ3(111) STGB, as shown in Figures 1(a) and (b).

We performed first-principles calculations for ferromagnetic bcc Fe Σ3(111) and nonmagnetic fcc Al(Cu) Σ5(012) STGBs. The electronic structure calculations and the atomic structure relaxations by force minimizations are performed using the Vienna Ab initio Simulation Package with the projector augmented wave method.[10–12] The generalized gradient approximation by Perdew, Burke, and Ernzerhof is used.[13] The calculations for iron system are done in spin-polarized (ferromagnetic) state (VOSKOWN = 0). The cutoff energy for the plane wave basis set is 280, 250, and 273 eV for Fe, Al, and Cu systems, respectively. The Monkhorst Pack k-point mesh is 8 × 4 × 1 for the unit cells, as shown in Figure 1. The Methfessel–Paxton smearing method with 0.1-eV width is used.

For the Fe case, the calculated energy of bcc Σ3(111) GB (γ_{gb}) is 1.52 J/m², and the energy of its fracture (111) surface (γ_s) is 2.69 J/m². Thus, the cohesive energy of the GB ($2\gamma_{int} = 2\gamma_s - \gamma_{gb}$) without segregation is 3.86 J/m². For the Al(Cu) case, the calculated energy of fcc Σ5(012) GB (γ_{gb}) is 0.57(0.86) J/m², and the energy of its fracture (012) surface (γ_s) is 1.01(1.55) J/m². The cohesive energy of the GB without segregation is 1.45(2.24) J/m² for Al(Cu).

B. *Calculations of the Work of Separation (Cohesive Energy) of GB*

We calculated the segregation energy of hydrogen at the GB in a similar manner as in Part I.[1] On the other hand, we calculated the cohesive energy of the GB in a different way. For the hydrogen case in this part, we assume that the segregated hydrogen atoms can diffuse a little on the gradually formed fracture surfaces. This

indicates that hydrogen can segregate at the most stable segregation site on the fracture surfaces by diffusing on the surface within a short distance. Furthermore, more hydrogen atoms can segregate on the gradually formed fracture surfaces coming from solid solution state, because the diffusion of hydrogen in bulk bcc Fe is very fast even at room temperature. The latter effect is called the "mobile" effect of hydrogen during fracture. In order to include these effects, we do not perform the tensile test calculations to calculate $2\gamma_{int}$ as in Part I.[1] Instead, we separately calculate the fracture-surface and GB segregation energies ($\Delta E_{FS,total}^{seg}$, $\Delta E_{GB,total}^{seg}$) for hydrogen atoms with varying the segregation density (using Eq. [7] in Part I[1]), and then calculate the cohesive energy using the following equation:

$$2\gamma_{int} = \left(2\gamma_s + \Delta E_{FS,total}^{seg,1}/A + \Delta E_{FS,total}^{seg,2}/A\right) - \left(\gamma_{gb} + \Delta E_{GB,total}^{seg}/A\right) \quad [1]$$

Here, A is the area of GB and surface plane (*ab* plane) of the unit cell. In this calculation, we divide the GB-segregated hydrogen atoms into the two groups of fracture-surface-segregated hydrogen atoms. In the case that five hydrogen atoms segregate at the GB plane in the unit cell ($\Delta E_{GB,total}^{seg}$) before fracture, for example, two hydrogen atoms are distributed on one fracture surface ($\Delta E_{FS,total}^{seg,1}$) and then the other three hydrogen atoms are distributed on the other fracture surface ($\Delta E_{FS,total}^{seg,2}$) after fracture so as to maximize the surface segregation energies in the system. In this method, hydrogen atoms can occupy the most stable segregation sites on the fracture surfaces after fracture; this means that the surface diffusion of hydrogen atoms on the fracture surfaces is allowed during fracture.

The preceding situation is that the number of total hydrogen atoms in the unit cell is assumed to be the same between the calculations of the fracture-surface segregation energy ($\Delta E_{FS,total}^{seg,1}$, $\Delta E_{FS,total}^{seg,2}$) after fracture and the GB segregation energy ($\Delta E_{GB,total}^{seg}$) before fracture. In this case, it is referred to as the immobile effect of hydrogen, although the surface diffusion effect of GB-segregated hydrogen atoms on the fracture surfaces is included. If the number of total hydrogen atoms in the calculations of fracture-surface segregation energy ($\Delta E_{FS,total}^{seg,1}$, $\Delta E_{FS,total}^{seg,2}$) after fracture is larger than that in the calculation of GB segregation energy ($\Delta E_{GB,total}^{seg}$) before fracture, in contrast, the diffusible effect of hydrogen coming from solid solution state to the gradually formed fracture surfaces during fracture is allowed in the calculation of $2\gamma_{int}$. In this case, the effect of the additional hydrogen atoms is referred as the mobile effect of hydrogen.

III. RESULTS AND DISCUSSION

A. *Segregation Energy of Hydrogen Atom in a Low Segregation Concentration*

We calculated the segregation (trapping) energy of hydrogen when one hydrogen atom is inserted at each atomic (interstitial) site in the unit cells. Here, the segregation energy of hydrogen is calculated with respect to the solid solution state. The solid solution state is separately calculated using another unit cell that does not include the GB. The calculated segregation energy at each interstitial atomic site is shown in Figure 2. For the Fe case (Figure 2(a)), we can see that the GB segregation energy ($\Delta E_{seg,atom}^{GB}$) of hydrogen at bcc Fe $\Sigma3(111)$ GB is about -0.45 eV/atom at most in a negative direction, while the surface segregation energy is about -0.78 eV/atom at most. From these results, we can see that the surface segregation energy is larger in a negative direction than the GB segregation energy, which is the same trend as the embrittling elements such as P and S, as shown in Part I.[1] Therefore, we can guess that hydrogen is also an embrittling element for Fe GB. For Al and Cu, the GB segregation energy of hydrogen is about -0.25 eV/atom at most in a negative direction, while the surface segregation energy is about -0.6 to -0.8 eV/atom at most. From these results, we can guess that hydrogen is also an embrittling element for Al and Cu GBs.

In Part I,[1] we used the McLean's equation curves to discuss the possibility of GB segregation of solute atoms from the calculated segregation energy. Similarly, we can discuss the possibility of hydrogen segregation at room temperature using the McLean's curve that is plotted at 300 K (27 °C), as shown in Figure 3. The segregation energy of hydrogen at bcc Fe $\Sigma3(111)$ GB is about -0.45 eV/atom at most, which is small in a negative direction compared with the GB segregation energy of B, C, P, and S (over -1.0 eV/atom), as stated in Part I.[1] For the hydrogen case, however, the segregation occurs at room temperature, about 300 K (27 °C) . In this temperature, the segregation energy of -0.45 eV/atom is very large in a negative direction, because 60 pct segregation (trapping) occurs even at 0.05 atomic parts per million (appm), 0.001 wt ppm for H, as can be seen from Figure 3.

The calculated solid solution energy and GB/fracture-surface segregation energies are summarized and compared with the experimental data in Table I and Figure 4. The experimental data include the zero-point energy, while the calculated data do not include it. However, the agreement between experiment and calculation seems to be good. The orders of size in the calculated solid solution energy for Fe, Al, and Cu are in good agreement with the experimental data. The calculated surface segregation energy of H on the Fe (100) surface is a little smaller than that on the Fe (111) surface, which does not agree with the experimental data. It may be due to the difference of the zero-point energy on Fe (100) and Fe (111) surfaces. For Al and Cu surfaces, we cannot find the experimental data of surface segregation energies of hydrogen for the (012) surface that we analyzed in our calculations. For the Cu case, we show the only available experimental data for the (311) surface instead of the (012) surface.

Although the experimental segregation energies of H at the Fe GB are not certain (from -0.10 to -0.61 eV/atom), these energies seem to be smaller in
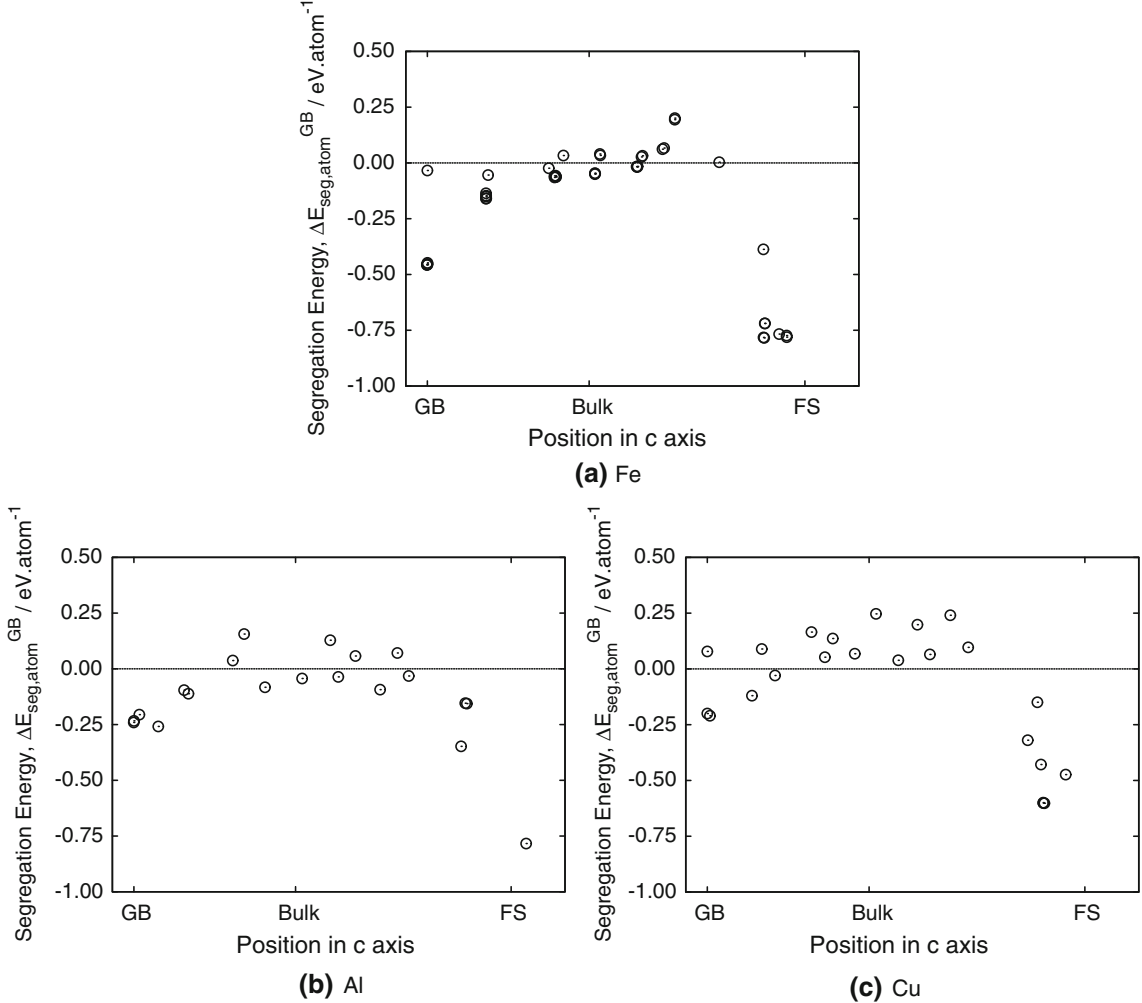
Fig. 2—Calculated segregation energies of hydrogen ($\Delta E_{\mathrm{seg,atom}}^{GB}$) when one hydrogen atom is placed at various interstitial sites in the cell, as shown in Fig. 1. The negative energy means stable state. GB indicates GB region, and *FS* indicates fracture (free) surface region. (*a*) Bcc Fe Σ3(111) GB cell, (*b*) fcc Al Σ5(012) GB cell, and (*c*) fcc Cu Σ5(012) GB cell.
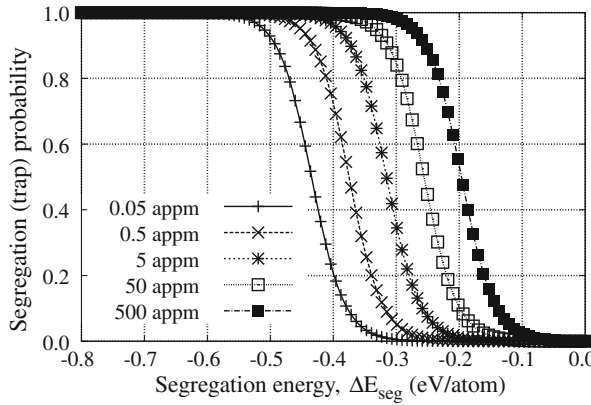

Fig. 3—Plotting of McLean's equation for hydrogen (H) segregation at 300 K (27 °C) (1 wppm H = 50 appm H).

a negative direction than the experimental surface segregation energy; this indicates that hydrogen is considered to be an embrittling element for iron.

An interesting trend is seen in the comparison between the energy of solid solution and fracture-surface/GB segregation energy for hydrogen in Fe, Al, and Cu, as shown in Figure 4. The embrittling potency energy of GB-segregated hydrogen can be defined as the energy difference between the fracture-surface- and GB-segregated energies of hydrogen, because this energy difference causes the reduction of the cohesive energy of GB, as stated in Part I.[1] From this figure, we can see that GB-segregated hydrogen has an embrittling effect for all Fe, Al, and Cu. On the other hand, the embrittling potency of H_2 gas is defined as the energy difference between the fracture-surface trapping state and H_2 gas state. For the Fe case, there is a large embrittling potency energy of H_2 gas. For the Al case, however, there is no embrittling potency energy of H_2 gas. For the Cu case, the embrittling potency energy of H_2 gas is small compared with the Fe case. These results indicate that H_2 gas embrittlement can occur for bcc Fe and fcc Cu, but does not occur for fcc Al. This is in good agreement with the experimental fact that Al shows the GB embrittlement by charged (inner) hydrogen, but

does not show H_2 gas (outer hydrogen) embrittlement even under the 85 MPa gaseous hydrogen condition.[18]

In summary, we find that solid solution hydrogen atom (charged hydrogen, inner hydrogen) can segregate at Fe, Al, and Cu GBs and on those fracture surfaces. It is interesting to note that gaseous hydrogen (H_2) can be trapped on the Fe and Cu fracture surfaces, but not on the Al fracture surfaces. This is consistent with the experimental fact that Al shows the GB embrittlement by charged hydrogen but not by gaseous hydrogen.[18]

B. Segregation Energy of Hydrogen Atoms with Increasing Segregation

We calculated the GB segregation energy of hydrogen with varying the segregation density ($\Delta E_{GB,\text{total}}^{\text{seg}}$). At each density of hydrogen segregation, we determined the most stable segregation configurations of hydrogen atoms that have the largest segregation energy in a negative direction. In Figure 5, we show the GB segregation energy of "total" hydrogen atoms in the unit cell ($\Delta E_{GB,\text{total}}^{\text{seg}}$) and the "incremental" segregation energy by adding one hydrogen atom ($\Delta E_{GB,\text{inc}}^{\text{seg}}$). If the incremental segregation energy is close to zero, there is not any more energy gain by hydrogen segregation; this indicates the segregation limit of hydrogen.

As shown in Figure 5, we can see that up to about six hydrogen atoms can segregate in the area of $A = 27.6$ Å^2 for bcc Fe $\Sigma3(111)$ GB. Similarly, about 12 hydrogen atoms can segregate in the area of $A = 37.3$ Å^2 for fcc Al $\Sigma5(012)$ GB, and about six hydrogen atoms can segregate in the area of $A = 29.2$ Å^2 for fcc Cu $\Sigma5(012)$ GB. In addition, we can see that the segregation energy of total hydrogen atoms in the cell becomes very large in a negative direction for Al, but small for Cu, compared with the Fe case. This indicates that the hydrogen atom easily segregates at Al GB up to a high density, while it has difficulty segregating at Cu GB, compared with Fe GB. This different behavior of hydrogen for Al and Cu in high segregation density is very interesting, because the behavior of the calculated segregation energy of hydrogen in low segregation density is quite similar for Al and Cu, as shown in Figures 2(b) and (c). This indicates that the interaction between segregated hydrogen atoms is quite different in Al and Cu GBs.

Next, we calculated the fracture-surface segregation energy of hydrogen with varying the segregation density

Table I. Experimental Data[14] and the Calculated Results for the Enthalpy (Energy) of Solution for H, the Largest Surface Segregation Energy of Hydrogen ($\Delta E_{\text{seg,atom}}^{FS}$) in a Negative Direction, and the Largest GB Segregation Energy of Hydrogen ($\Delta E_{\text{seg,atom}}^{GB}$)

	Experiment* (eV/atom H)	This Work (Calculation) (eV/atom H)
Energy of solution in bcc Fe	0.30	0.22
fcc Al	0.70	0.84
fcc Cu	0.43	0.52
$\Delta E_{\text{seg,atom}}^{FS}$** on Fe(100)	−0.82	−0.62
Fe(111)	−0.75	−0.79
Al(012)	—	−0.78
Cu	−0.63 for (311)	−0.64 for (012)
$\Delta E_{\text{seg,atom}}^{GB}$ in Fe	−0.1, −0.51, −0.61[†]	−0.45 for $\Sigma3(111)$

*Experimental data include the zero-point energy of hydrogen, which is not included in this work (calculation).

**Experimental surface segregation energy is estimated as the sum of the enthalpy of solution and the adsorption energy of H_2 on the surface.

[†]−0.1: Ref. 15, −0.51: Ref. 16, −0.61: Ref. 17.

Fig. 4—Comparison in energy among four states: (1) solid solution, (2) H_2 gas, (3) GB segregation, and (4) fracture-surface segregation, in the case of a low segregation density of hydrogen atom. This figure implies that the embrittlement occurs by inner (solid solution) hydrogen and by outer hydrogen (H_2 gas) for bcc Fe GB, while the embrittlement occurs by inner hydrogen but does not occur by outer hydrogen for fcc Al GB.
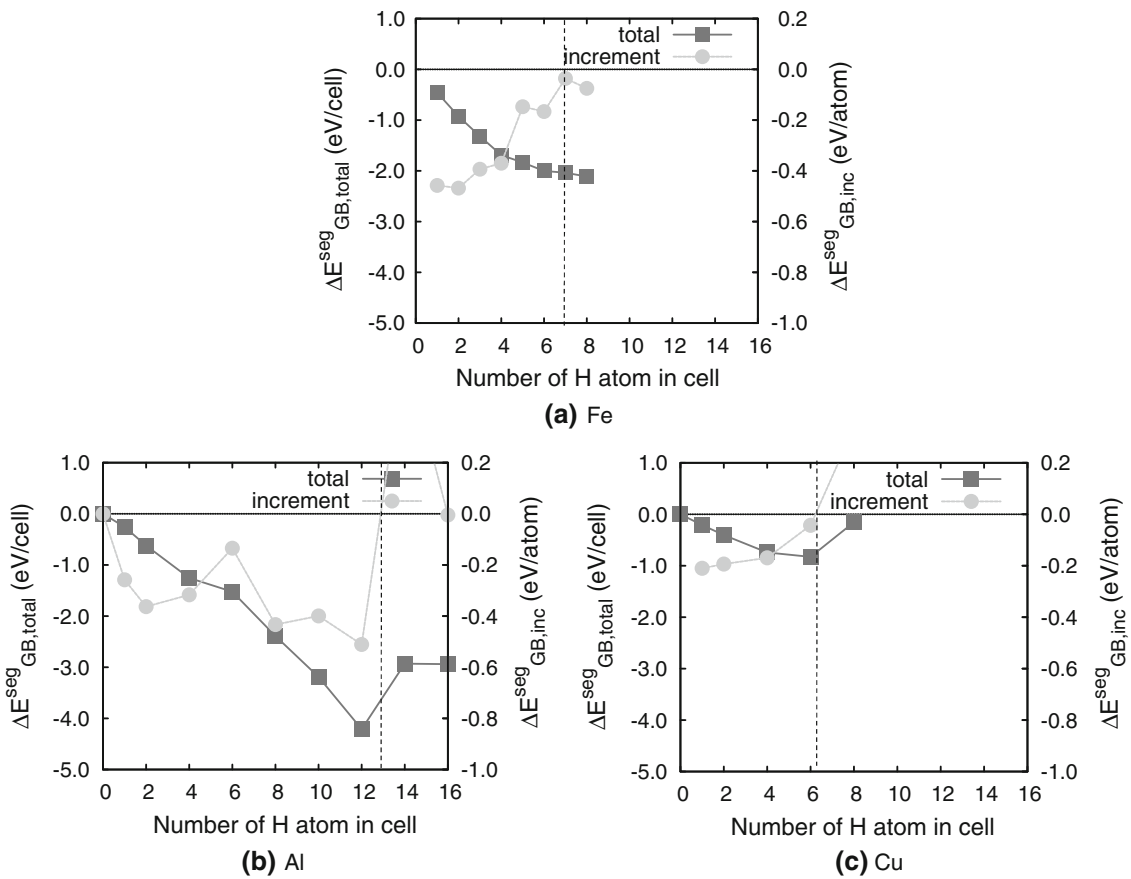
Fig. 5—Calculated GB segregation energies ($\Delta E_{GB,total}^{seg}$) of hydrogen atoms with varying the segregation density for (*a*) bcc Fe $\Sigma3(111)$ GB, (*b*) fcc Al $\Sigma5(012)$ GB, and (*c*) fcc Cu $\Sigma5(012)$ GB. "Total" line indicates the segregation energy for total hydrogen atoms in the GB of the unit cell. The area of the GB plane in the unit cell is equal to A ($A = 27.6$ Å^2 for Fe, 37.3 Å^2 for Al, and 29.2 Å^2 for Cu). "Increment" line ($\Delta E_{GB,inc}^{seg}$) indicates the incremental segregation energy by adding one hydrogen atom. Dashed lines roughly indicate the GB segregation limit of hydrogen atoms in the area of A.

of hydrogen ($\Delta E_{FS,total}^{seg}$, $\Delta E_{FS,inc}^{seg}$). The calculated results are shown in Figure 6 for Fe, Al, and Cu cases. The trends in the comparison among Fe, Al, and Cu are similar with GB segregation cases. The segregation limit on one fracture surface is also similar to the GB case. On the (111) fracture surface of bcc Fe ($A = 27.6$ Å^2), about six hydrogen can segregate at most. On the (012) Al surface ($A = 37.3$ Å^2), more than eight hydrogen atoms can segregate. Furthermore, hydrogen segregated on Al surface may become H$_2$ gas, because the H$_2$ gas state is more stable than the segregation state on the Al(012) surface, as shown in Figure 4. On the (012) Cu surface ($A = 29.2$ Å^2), only about four hydrogen atoms can segregate at most. From these results, we can understand that the segregation limit of hydrogen atom after fracture becomes almost twice compared with that before fracture, because the area of fracture surfaces after fracture ($2A$) is twice compared with the area of GB before fracture (A).

C. Cohesive Energy of the GB with Hydrogen Segregation

From the separately calculated GB and fracture-surface segregation energies of hydrogen ($\Delta E_{GB,total}^{seg}$,

$\Delta E_{FS,total}^{seg}$), as shown in Figures 5 and 6, we estimated the change in the cohesive energy of GB, $2\gamma_{int}$, by hydrogen segregation using Eq. [1]. Here, the GB-segregated hydrogen atoms are divided into the two fracture surfaces so as to maximize the fracture-surface segregation energy in a negative direction. For an example, when six hydrogen atoms segregate at the GB, three hydrogen atoms are distributed to one fracture surface and then the remaining three hydrogen atoms are distributed to the other fracture surface; this gives the largest surface segregation energy in total. The calculated results of $2\gamma_{int}$ are shown in Figure 7. We can see that up to the GB segregation limit (denoted by dashed lines in Figure 7), the $2\gamma_{int}$ decreases by about 40 pct for the Fe case, by more than 90 pct for the Al case, and by about 50 pct for the Cu case. Although the maximum decreases of $2\gamma_{int}$ for Fe and Cu cases are similar size with each other, it should be remembered that hydrogen atoms are considered to be very difficult to segregate at Cu GB compared with Fe GB, as can be seen from the GB segregation energies, as shown in Figure 5.

In the discussion so far, the number of segregated hydrogen atoms is assumed not to change during fracture; the number of hydrogen atoms segregated at
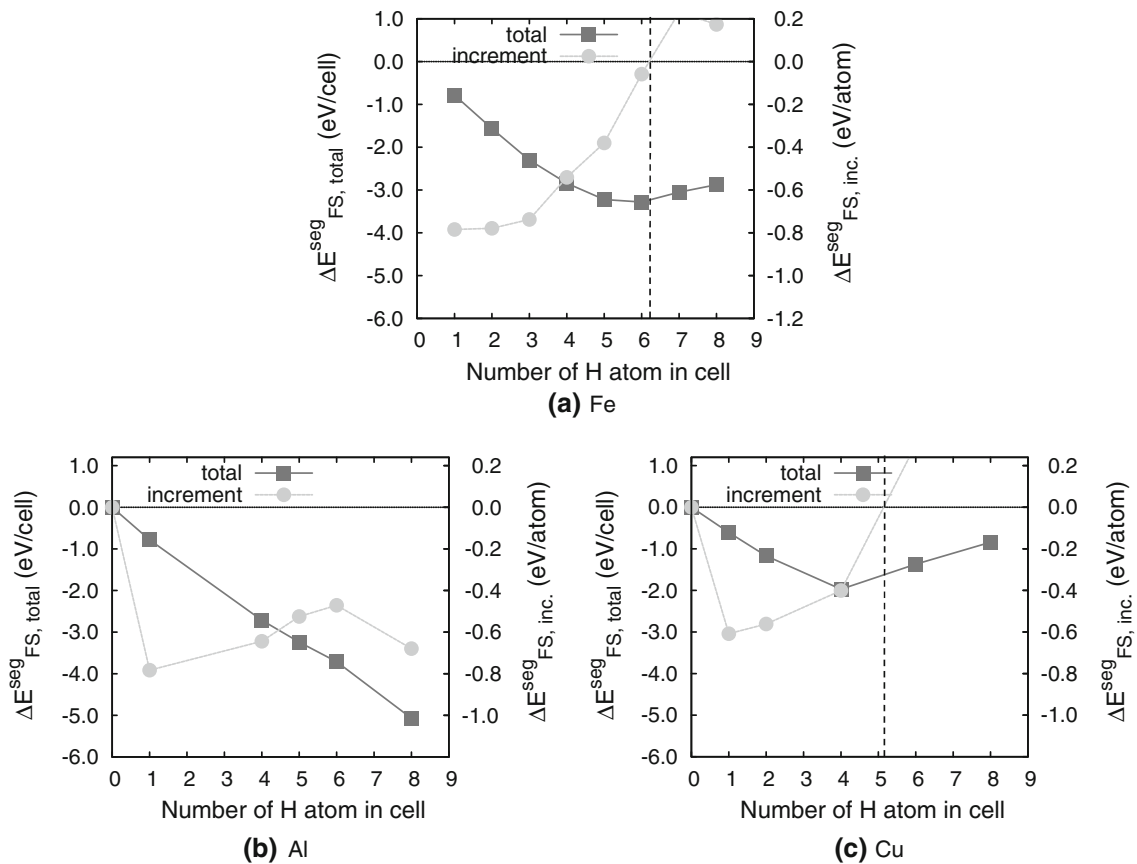
Fig. 6—Calculated surface segregation energies ($\Delta E_{FS,\text{total}}^{\text{seg}}$) of hydrogen atoms with varying segregation density for (*a*) bcc Fe (111) surface, (*b*) fcc Al (012) surface, and (*c*) fcc Cu (012) surface. "Increment" line ($\Delta E_{FS,\text{inc}}^{\text{seg}}$) indicates the incremental segregation energy by adding one hydrogen atom. Dashed lines roughly indicate the surface segregation limit of hydrogen atoms in the area of A for one fracture surface in the unit cell.

GB before fracture and that on the two fracture surfaces after fracture are assumed to be the same. However, this assumption may not be correct for the hydrogen case, especially for the iron system, because the diffusion of hydrogen is very fast even at room temperature and the diffusion may become comparable to the crack growth velocity. For this reason, we estimated this mobile effect of hydrogen during fracture for the bcc Fe $\Sigma 3(111)$ GB case. One possible factor is that the diffusible hydrogen atoms coming from solid solution state segregate on the gradually formed fracture surfaces during fracture. This effect is calculated and shown in Figure 8(a). Another possible factor is that the gasified hydrogen (H_2 molecule) in the crack opening space is adsorbed on the gradually formed fracture surfaces. This effect is also calculated and shown in Figure 8(b). In both two cases, the cohesive energy of the GB can be significantly reduced, as can be seen in Figure 8. Hereafter, we focus on the mobile effect of solid solution hydrogen.

We estimated the superposition of the immobile and mobile effects of hydrogen on the reduction of $2\gamma_{\text{int}}$, as shown in Figure 9. In this figure, we assume that six hydrogen atoms have already segregated at the GB plane (area $A = 27.6$ Å^2) of the unit cell including bcc Fe $\Sigma 3(111)$ GB, and then the mobile effect of solid solution hydrogen, as shown in Figure 8(a), is added. By

the superposition of the two effects, the immobile and mobile effects of hydrogen, the cohesive energy of bcc Fe $\Sigma 3(111)$ GB is reduced by 60 to 70 pct at most, as shown in Figure 9. Recently, Wang *et al.*[19] showed that the fracture stress of high-strength steel was reduced by about 80 pct at most with increasing diffusible hydrogen content in the slow strain rate test; the amount of fracture stress reduction is in agreement with the reduction of the cohesive energy in our calculations. In addition, Wang *et al.* have shown that the fracture stress reduction is saturated at 80 pct with increasing hydrogen content (Figure 9 in Reference 19). From our calculations, this saturation can be understood to be caused by the fact that there is the density limit of hydrogen segregation on the fracture surfaces, as shown in Figure 6(a).

We suggest a new idea regarding the origin of the upper and lower critical stresses that are observed in the constant-load test of delayed fracture induced by hydrogen in high-strength steels. Looking at the calculated reduction of $2\gamma_{\text{int}}$, as shown in Figure 9, we can find an important behavior that can explain the origin of upper and lower critical stresses. The immobile effect of hydrogen atoms that have already segregated at GB before fracture reduces the GB cohesive energy ($2\gamma_{\text{int}}$) by about 40 pct at most. In this case, the delay time for
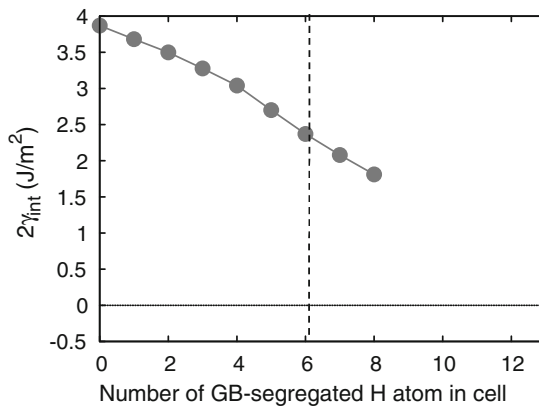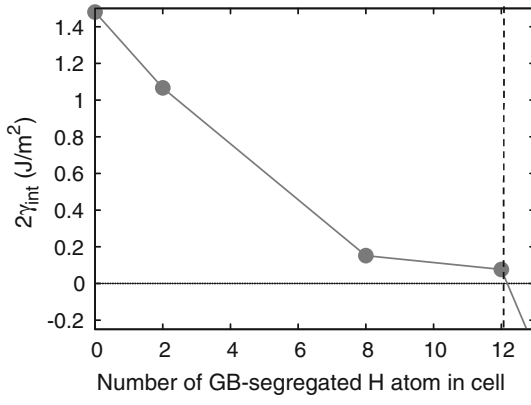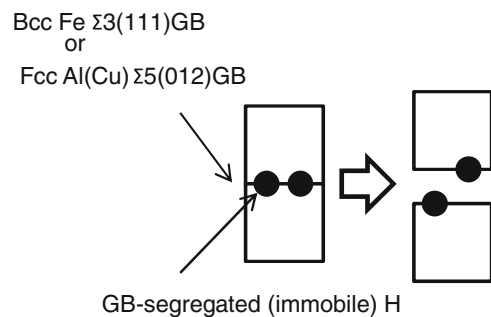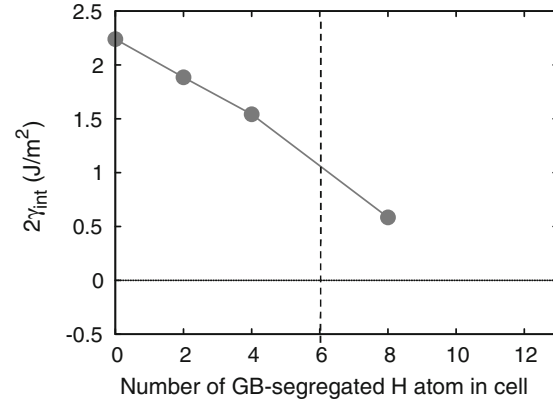
Fig. 7—Change of the cohesive energy ($2\gamma_{int}$) of (a) bcc FeΣ3(111) GB, (b) fcc Al Σ5(012) GB, and (c) fcc Cu Σ5(012) GB by the GB-segregated hydrogen atoms ("immobile" effect of hydrogen, as shown in the schematic illustration). Dashed lines indicate the GB segregation limit of hydrogen atoms in the area of A (27.6 Å^2 for Fe, 37.3 Å^2 for Al, and 29.2 Å^2 for Cu).
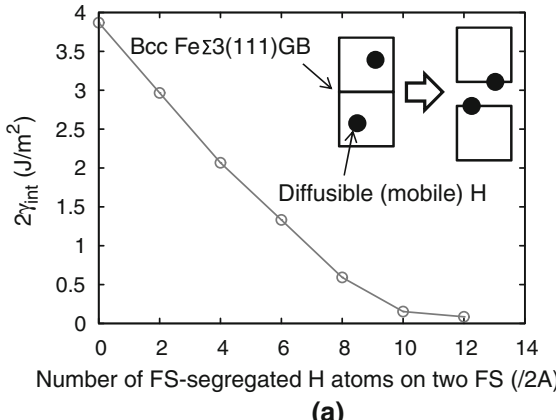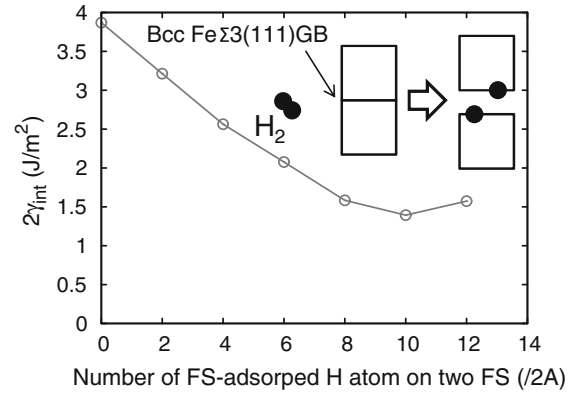

Fig. 8—The reduction of the cohesive energy $2\gamma_{int}$ of bcc Fe Σ3(111) GB by the mobile effect of hydrogen (a) from inner bulk (solid solution state) to (111) fracture surfaces (FS) and (b) from hydrogen gas state (H$_2$ molecule) to (111) fracture surfaces. The schematic illustrations to understand these two effects are shown in the graphs.

fracture after the incubation period (microcrack initiation) is not necessary. On the other hand, the delay time is necessary for the crack propagation by the mobile effect of hydrogen atoms, which come from solid solution state to the gradually formed fracture surfaces and then segregate on the fracture surfaces. From these

considerations, we suggest a new idea about the origin of the upper and lower critical stresses; the upper critical stress is determined by the amount of hydrogen atoms, which are already segregated at GBs before fracture (before crack propagation starts), and the lower critical stress is determined by the total amount of immobile
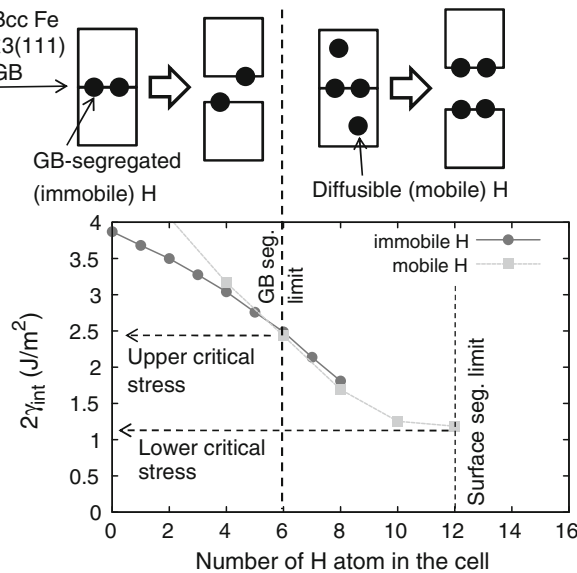
Fig. 9—Reduction of the cohesive energy ($2\gamma_{int}$) of bcc Fe Σ3(111) GB with varying trapping (segregation) density of hydrogen atoms at GB and its two fracture surfaces. The reduction in the cohesive energy by the GB-segregated hydrogen is referred to as "immobile H," which is the same plotting as Fig. 7(a).The reduction by the mobile effect of hydrogen that moves from solid solution state to fracture surface during fracture is referred to as "mobile H," which is the same plotting as Fig. 8(a) but is connected at 6 H atoms (GB segregated limit) with the line of immobile hydrogen effect. In this case, the upper critical stress is determined by six GB-segregated hydrogen atoms, and the lower critical stress is determined by 12 surface-segregated hydrogen atoms. The schematic illustrations are shown above the graph to understand these immobile and mobile effects of hydrogen.

and mobile hydrogen atoms, the latter of which segregate additionally on the gradually formed fracture surfaces during fracture (crack propagation) coming from solid solution state (or H_2 gas in the crack opening space).

Finally, we show our preliminary calculated results for the reduction of the cohesive energy of (100) cleavage plane of bcc Fe by the adsorption of hydrogen gas (H_2 molecule) in Figure 10. We calculated this energy reduction using the cell including two (100) planes. The cohesive energy of the (100) plane is reduced by 25 to 30 pct at most with increasing adsorption of hydrogen from H_2 gas. This indicates that hydrogen gas environment can enhance the cleavage crack propagation at the bcc Fe (100) plane, and it is consistent with the experimental result; the (100) cleavage crack in Fe-2.6 pct Si single crystal can be enhanced by H_2 gas environment.[20] The details of calculations will be published elsewhere.[21]

IV. SUMMARY

We calculated the cohesive energy $2\gamma_{int}$ of bcc Fe Σ3(111) and fcc Al(Cu) Σ5(012) symmetrical tilt GBs with varying the segregation density of hydrogen. Within the immobile effect of hydrogen, the calculated $2\gamma_{int}$ is decreased by about 40, 90, and 50 pct at the
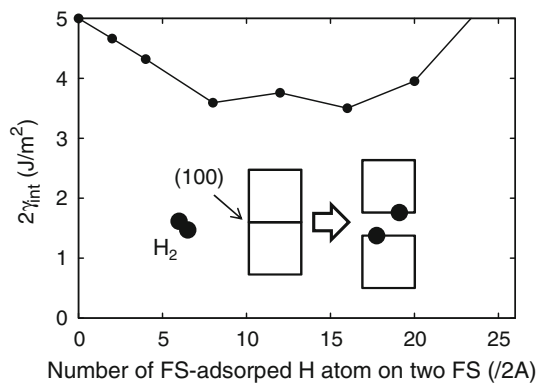

Fig. 10—The calculated reduction of the cohesive energy of (100) cleavage plane of bcc Fe by the adsorption of hydrogen gas (H_2 molecule). In this case, $2\gamma_{int} = 2\gamma_{cleavage} = 2\gamma_s$ because $\gamma_{gb} = 0$. The area of (100) plane (A) is 32.08 Å^2. The surface energy of (100) plane (γ_s) is 2.5 J/m^2. The schematic illustration is shown to understand the effect of hydrogen gas (H_2) in the graph.

segregation density limit of hydrogen atoms at the GBs for Fe, Al, and Cu cases, respectively. The segregation density limit is defined as the density at which the incremental segregation energy is about zero. These results indicate that hydrogen-induced GB embrittlement for Fe, Al, and Cu may be caused by the reduction of $2\gamma_{int}$, which is the same mechanism as the embrittlement by phosphorous and sulfur segregation, as stated in Part I.[1]

The amount of hydrogen atoms segregated on the two fracture surfaces ($2A$) after fracture can be larger than that segregated at the GB area (A) before fracture in Eq. [1], because the bulk diffusion of hydrogen atom is very fast at room temperature, especially for the Fe case. This is called the mobile effect of hydrogen during fracture, as suggested by Rice and Wang.[2] This mobile effect of hydrogen is estimated by using the calculated fracture-surface segregation energy of hydrogen coming from solid solution state in bulk for the Fe case. While the immobile effect of hydrogen can decrease $2\gamma_{int}$ by about 40 pct at most, the addition of the mobile effects of hydrogen can decrease the $2\gamma_{int}$ by about 70 to 80 pct at most. From these considerations, we suggest a new idea about the origin of the upper and lower critical stresses observed in the constant-load test of hydrogen-induced delayed fracture in high-strength steels; the upper critical stress is determined by the amount of GB segregated (immobile) hydrogen atoms before fracture, and the lower critical stress is determined by the amount of the immobile and mobile hydrogen atoms, the latter of which is the fracture-surface segregated hydrogen atoms during fracture coming from solid solution state or H_2 gas in the crack opening space.

Another aspect of the mobile effect of hydrogen is the reduction of $2\gamma_{int}$ by the adsorption of hydrogen gas (H_2 molecule) instead of solid solution hydrogen. We estimated the reduction of surface energy by hydrogen trapping on the (100) fracture surfaces from H_2 gas molecule, and found that a significant reduction by 25 to 30 pct occurs in the cohesive energy ($2\gamma_{cleavage} = 2\gamma_s$) of (100) cleavage plane in bcc Fe. This indicates that the

enhancement of (100) cleavage of bcc Fe can occur in the environment of H_2 gas, which is in agreement with experiments.

REFERENCES

1. M. Yamaguchi: *Metall. Mater. Trans. A*, 2010, vol. 41A, DOI: 10.1007/s11661-010-0381-5.
2. J.R. Rice and J.-S. Wang: *Mater. Sci. Eng.*, 1989, vol. A107, pp. 23–40.
3. J.P. Hirth: *Metall. Trans. A*, 1980, vol. 11A, pp. 861–90.
4. L. Zhong, R. Wu, A.J. Freeman, and G.B. Olson: *Phys. Rev. B*, 2000, vol. 62, pp. 13938–41.
5. M. Iwamoto and Y. Fukai: *Mater. Trans. JIM*, 1999, vol. 40, pp. 606–11.
6. Y. Tateyama and T. Ohno: *Phys. Rev. B*, 2003, vol. 67, pp. 174105–14.
7. G. Lu and E. Kaxiras: *Phys. Rev. Lett.*, 2005, vol. 94, pp. 155501–04.
8. M. Yamaguchi, K. Ebihara, M. Itakura, T. Kadoyoshi, T. Suzudo, and H. Kaburaki: *Proc. Int. Conf. for Processing and Fabrications of Advanced Materials 18* (*PFAM18*), Sendai, Japan, 2009, vol. 1, pp. 65–74.
9. A. Troiano: *Trans. ASM*, 1960, vol. 52, pp. 54–80.
10. G. Kresse and J. Hafner: *Phys. Rev. B*, 1993, vol. 47, pp. 558–61.
11. G. Kresse and J. Furthmueller: *Phys. Rev. B*, 1996, vol. 54, pp. 11169–86.
12. G. Kresse and D. Joubert: *Phys. Rev. B*, 1999, vol. 59, pp. 1758–75.
13. J.P. Perdew, K. Burke, and M. Ernzerhof: *Phys. Rev. Lett.*, 1996, vol. 77, pp. 3865–68.
14. K. Christmann: *Surf. Sci. Rep.*, 1983, vol. 9, pp. 1–163.
15. W.Y. Choo and J.Y. Lee: *Metall. Trans. A*, 1982, vol. 13A, pp. 135–40.
16. K. Ono and M. Meshii: *Acta Metall. Mater.*, 1992, vol. 40, pp. 1357–64.
17. T. Asaoka, C. Dagbert, M. Aucouturier, and J. Galland: *Scripta Metall.*, 1977, vol. 11, pp. 467–72.
18. K. Ichitani and S. Osaki: *Proc. 18th Int. Symp. on Processing and Fabrication of Advanced Materials* (*PFAM XVIII*), Sendai, Japan, 2009, vol. 1, pp. 55–64.
19. M. Wang, E. Akiyama, and K. Tsuzaki: *Corr. Sci.*, 2007, vol. 49, pp. 4081–97.
20. H. Vehoff and W. Rothe: *Acta Metall.*, 1983, vol. 31, pp. 1781–93.
21. M. Yamaguchi: unpublished research, 2009.